Journal of Molecular Structure 1221 (2020) 128873

Contents lists available at ScienceDirect

Journal of Molecular Structure

journal homepage: www.elsevier.com/locate/molstr

Structural, thermal, spectroscopic, electronic and biological activity properties of coumarin-153 dyes for DSSCs: A DFT benchmark study

Y. Erdogdu[a,*], U.C. Baskose[b], S. Saglam[a], M. Erdogdu[c], H. Ogutcu[d], S Özçelik[a,b]

[a] Department of Physics, Gazi University, Ankara, Turkey
[b] Photonics Application and Research Center, Gazi University, Ankara, Turkey
[c] Landscape Architecture, Kırsehir Ahi Evran University, Kırşehir, Turkey
[d] Department of Field Crops, Kırsehir Ahi Evran University, Kırşehir, Turkey

ARTICLE INFO

Article history:
Received 12 February 2020
Revised 24 June 2020
Accepted 9 July 2020
Available online 10 July 2020

Keywords:
Coumarin-153
Density functional theory (DFT)
Vibrational spectroscopy
Anti-microbial activity

ABSTRACT

The structural, thermal, spectroscopic, electronic and biological activity properties of the Coumarin-153 molecule report herein a joint experimental and theoretical investigation. Fourier Transform Infrared (FT-IR), Nuclear Magnetic Resonance (NMR) and Ultra Violet (UV) spectroscopy are used to probe the spectroscopic properties of the Coumarin-153 molecule. Theoretical vibrational, NMR and UV–Vis spectroscopic, structural and some electronic properties of Coumarin-153 molecule were estimated by Density Functional Theory (DFT). In the DFT calculations, the B3LYP functional with 6–311G(d,p) basis sets were applied to carry out the quantum mechanical calculations. Some features just mentioned were visualized. In addition, Coumarin-153 molecule was also evaluated for antibacterial and antifungal activities against pathogenic bacteria (Gram negative and Gram positive) and yeast.

1. Introduction

Coumarins are the photoactive organic molecule used in the synthesis of Dye-Sensitized Solar Cells (DSSC). Photoactive organic dyes are very effective in light absorption and light electrical conversion in dye-sensitized solar cells [1,2]. In today and in future studies, achieving optimum device efficiencies in dye-sensitized solar cells and extending the stable cell lifetime are priority issues to be addressed [3]. The efficiency of a solar cell can be predicted by determining some parameters such as the open circuit voltage and the short circuit current density. These parameters are related to the molecular structure and to the HOMO and LUMO of the photoactive organic dyes materials. These materials constitute the core of the photovoltaic device [4].

According the structure and working principle of dye-sensitized solar cell (DSSC), photovoltaic cycle is completed with absorption of light, decomposition of charges, charge transfer and collection of charges. The detailed study of kinetic and dynamics of charge motion within this system is very important for the development of organic and dye sensitized solar cells technology. Also, the photon absorption process, the maximum absorption wavelength and the band gap energy of the photoactive organic dyes materials is important for the synthesis of DSSC. The much more characterization is needed in order to propose TiO_2- Coumarin-153 hybrids as good candidates for the development of efficient dye-sensitized solar cells. Thus, theoretically explaining the UV–Vis spectra could be an important step in the design of organic solar cells [4]. These results show that the present model could be useful for the evaluation of reliable molecular structure and properties values for systems of interest in materials science frameworks, which could be relevant for organic photovoltaic applications [4].

The DSSC consists of an electrolyte, a photo-active dye, an oxide semiconductor electrode, and a metal-conducting electrode. In the literature, transparent conductive oxide (TCO) materials, which are mostly fluorine doped tin oxide (FTO) and indium tin oxide (ITO) coated glass, are used as a substrate in the production of dye-sensitized solar cells. Nano-crystalline TiO_2, ZnO and SnO_2 films, which can be obtained by different methods as semiconductor oxide, are the most frequently used materials. For the counter electrode, pure metals such as platinum (Pt) gold (Au) and silver (Ag) are the most commonly used materials. Iodide-triiodide (I_3^--I^-) as liquid electrolyte; ionic liquids and polymer gel containing redox couples as semi-solid electrolyte; inorganic p-type materials and organic polymers are used as solid state electrolytes. Ruthenium complex polypyridyl dyes, metal-free organic dyes, porphyrin dyes, quantum dot sensitizers, perovskite based sensitizers are used as sensitizing materials [5–8].

In addition to the discussions above about Coumarin and its derivatives, they are a member of the benzopyrones family. They

* Corresponding author.
E-mail address: yerdogdu@gazi.edu.tr (Y. Erdogdu).

https://doi.org/10.1016/j.molstruc.2020.128873
0022-2860/

have a wide range of biological activities and behaviors [10]. The source of their biological activity is their structural properties. These structural properties are correlated to their physicochemical properties. Over the past decade, Coumarin and its derivatives have attracted increasing interest in pharmaceuticals [11], fluorescence sensors [12], chemoreceptors [13] and precursors for the synthesis of coumarin pyrazoles [14]. Some coumarin and derivatives have also anticoagulants, antioxidants, antidepressants, analgesics and diagnostics [15] properties. Coumarin derivatives containing a substituted hydroxyl group possess antibiotic and antifungal activities.

In the present work, Coumarin-153 has been investigated by using density functional theory and spectroscopic methods. Vibrational, structural and some electronic properties of Coumarin-153 were investigated by experimental and theoretical methods. Note that the infrared, NMR and UV–Vis spectra of Coumarin-153 molecule, which haven't been assigned yet, performed the complete assignment. To understand the vibrational and some electronic properties of Coumarin-153 molecule, as an important compound in the scientific research, the FT-IR, NMR and UV–Vis spectra of Coumarin-153 have detected and evaluated computational results. In addition, Coumarin-153 molecule was evaluated for antibacterial and antifungal activities.

2. Materials and methods

All the theoretical process and calculations were performed with the Gauss View 5.0 [16] and Gaussian 09 W [17] quantum chemistry package programs by used DFT/B3LYP [18] functional and 6–311G(d,p) [19] basis set. The vibrational assignments were accomplished by means of the potential energy distribution (PED). The results of PED were determined by using of scaled quantum mechanics (SQM) program [20].

Coumarin-153 molecule was provided from Sigma-Aldrich. The FT-IR spectrum of Coumarin-153 was recorded by Bruker Vertex 80 FTIR spectrometer. In the FT-IR spectra, spectral region is 4000–550 cm^{-1}, the spectral resolution is 4 cm^{-1} and scan is 32. UV–Vis absorption spectra of Coumarin-153 was detected by Lambda 2S, Perkin Elmer UV–Vis spectrometer. This experiment was realized at RT in the range of 200–1100 nm. In the UV–Vis experiment, methanol was used as a solvent. ^{1}H and ^{13}C NMR spectral data were detected by means of Bruker Avance 300 MHz spectrometer in Chloroform solution.

The antimicrobial activity of Coumarin-153 molecule determined. The well-diffusion method was used for antimicrobial studies. In this studies, Authors were used the five Gram-negative bacteria (*S. typhi* H NCTC901.8394, *E. coli* ATCC1280, *Klebsiella pneumonia* ATCC 27,853, *Proteus vulgaris* RSKK 96,026, *Pseudomonas putida),* four Gram-positive bacteria (*Staphylococcus aureus* ATCC25923, *Staphylococcus epidermis* ATCC12228, *Micrococcus luteus* ATCC9341, *Bacillus cereus* RSKK-863) and one yeast (*Candida albicans* Y-1200-NIH) [21–26].

The Coumarin-153 molecule was kept dry at room temperature and dissolved (0.25 μg/ml) in DMF. DMF was used as solvent for Coumarin-153 molecule and control. Pathogenic bacteria and yeast cultures were placed in sterile petri dishes for 1% (v/v) of 24 h. These cultures were containing 10^6 CFU/mL. Then, sterile Mueller-Hinton Agar (MHA) (15 mL) was sheds into the petri dishes and allowed to solidity. After solidification, wells with a diameter of 6 mm were drilled carefully using a sterile cork borer and completely filled with Coumarin-153. Finally, plates were incubated for 24 h at 37 °C on the incubator. At the end of incubation, the zone of growth inhibition of each sample determined by using the average value of the two wells [27–29]. The pathogenic bacteria and yeast were also tested for resistance to five antibiotics produced by Oxoid Lt., Basingstoke, UK (Ampicillin, Nystatin, Kanamycin, Sulphamethoxazol, Amoxycillin) [30–32].

3. Results and discussion

3.1. Optimization of molecular geometry

The energies of the optimized geometry was worked by using B3LYP and 6–31 G(d,p) basis set for various possible conformers of Coumarin-153. There are about two conformers obtained for Coumarin-153. The optimized energy value and molecular geometry of the possible conformers of Coumarin-153 were shown in Fig. 1. It is clear in Fig. 1, the optimizations were shown that the conformer-1 produced the global minimum. When examining the energy differences between the conformer-1 and conformer-2 (see Figure 1), it is seen that the relative energies of the conformer-2 were less than kT energy (0.6 kcal/mol at room temperature and 1 atm pressure). It is note that conformer-2 have considerable population at room temperature. The quantum chemical analysis of Coumarin-153 will do over all the conformers.

The molecular geometry of Coumarin-153 molecule was illustrated in Fig. 2 with the atomic numbering in the ground state. Its geometric parameters were gathered in Table S1. The calculated geometrical parameters were compared with those of X-Ray study [33].

The bond angles between the pyrone and benzene rings of the conformer-1 (conformer-2) Coumarin-153 molecule were obtained at 115.8° (116.0°) /115.6° for $C_8–C_9–O_1$, 126.1° (126.1°) /126.7° for $C_5–C_{10}–C_4$ and 123.4° (123.4°) /122.5° for $C_9–O_1–C_2$ by means of DFT/X-Ray process. The conformer-1 (conformer-2) of the dihedral angles between the rings mentioned above of the Coumarin-153 molecule were determined at 179.9° (179.9°) /176.8 ($C_5–C_{10}–C_4–C_3$) and 179.7° (179.8°) /177.3° ($C_5–C_{10}–C_9–O_1$) for DFT/X-ray data. This apparently shows that the pyrone and benzene rings of the Coumarin-153 molecule has planar geometry.

The average C-F bond length of the trifluoromethyl group in the Coumarin-153 molecule were determined about 1.333 Å by X-Ray experimental process [33]. Yip et al. [33] reported that the F-C-F and F-C-C bond angles have been experimentally founded at 106.2° and 112.5°, respectively. In the present study, the C-F bond length and the F-C-F and F-C-C bond angles were theoretically predicted at 1.349 Å, 106.9° and 111.8°, respectively. From Table S1, It is note that theoretical computed geometric parameters were close to those of X-Ray study.

3.2. Vibrational analysis

The Coumarin-153 molecule possesses C_1 point group symmetry and has 36 atoms ($C_{16}H_{14}F_3NO_2$) with 102 normal modes. All the vibrations are active in IR spectra. The experimental FT-IR spectra of Coumarin-153 molecule is shown in Fig. 3. The corresponding predicted FT-IR spectra is given Fig. 3. The observed and predicted wavenumbers, their relative intensities, total energy distributions of Coumarin-153 molecule are gathered in Table 1.

The typical CH stretching vibrations of the hetero-aromatic structure are appeared in 3054–3072 cm^{-1} frequency ranges [34]. One band experimentally obtained at 3072 cm^{-1} are defined as the CH stretching vibration of Coumarin-153. In accordance with the observed wavenumber, this band was predicted at 3098 cm^{-1} (conformer-1) and 3099 cm^{-1} (conformer-2) by DFT. The CH_2 stretching vibrations were measured lower than that of CH stretching vibration. The CH_2 stretching vibration bands observed at 2842 cm^{-1}, 2875 cm^{-1}, 2891 cm^{-1}, 2933 cm^{-1}, 2952 cm^{-1} in the FT-IR spectra. The bands detected at 2933 cm^{-1} and 2952 cm^{-1} were assigned to the asymmetric stretching vibrations by means of PED. At the same time, 2842 cm^{-1}, 2873 cm^{-1} and 2891 cm^{-1} bands determined as the symmetric CH_2 stretching vibrations.

On the basis of physical state, electronic mass effects of neighboring substituents, conjugations and hydrogen bonding, the $C = O$

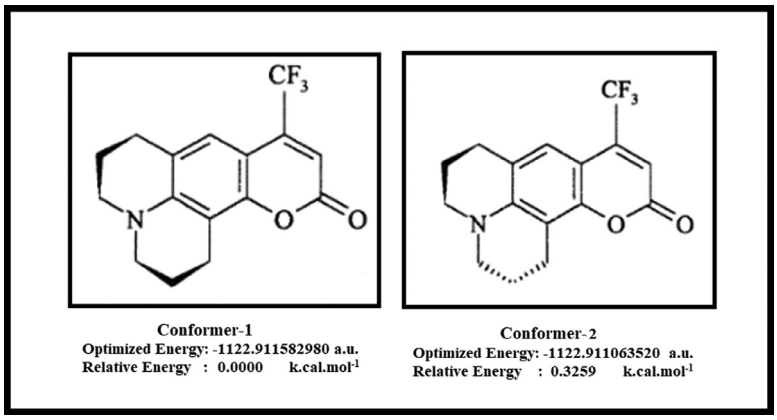

Fig. 1. . The optimized energies and geometries of conformers of Coumarin-153.

Table 1
Some selected vibrational spectral data of Coumarin-153 compound.

	Theoretical				Experimental	
	Conformer-1		Conformer-2		FT-IR	PED
	Freq[a]	I_{IR}^{b}	Freq[a]	I_{IR}^{b}		
ν_{27}	550	0.610	562	0.818	561	$\delta_{HCH}(46\%)+\delta_{CCH}(21\%)$
ν_{28}	571	0.944	579	0.779	570	$\tau_{CCCC}(32\%)+\gamma_{CCH}(20\%)+\delta_{HCH}(12\%)+\tau_{CNCH}(10\%)$
ν_{29}	606	0.356	603	0.517	588	$\delta_{HCH}(41\%)+\tau_{CCCC}(17\%)+\tau_{CNCH}(11\%)$
ν_{30}	632	0.204	633	0.195	622	$\gamma_{CCH}(26\%)+\tau_{CCCC}(24\%)+\tau_{CCCO}(13\%)$
ν_{31}	652	3.042	648	1.926	644	$\delta_{HCH}(32\%)+\delta_{CCC}(19\%)$
ν_{32}	677	1.326	675	1.426	667	$\tau_{CCCC}(34\%)+\tau_{CCCH}(21\%)+\tau_{CCCF}(10\%)$
ν_{33}	692	0.155	692	0.130	692	$\tau_{CCCC}(33\%)+\gamma_{CCH}(25\%)$ (R1)
ν_{35}	716	1.276	712	1.697	709	$\delta_{HCH}(31\%)+\delta_{CCH}(24\%)+\delta_{FCF}(18\%)$
ν_{36}	736	1.303	740	1.017	738	$\tau_{CCCC}(47\%)+\delta_{CCH}(17\%)+\delta_{HCH}(14\%)$
ν_{37}	792	1.275	791	1.296	757	$\delta_{CCO}(35\%)+\delta_{CCH}(21\%)+\delta_{HCH}(15\%)$ (R1)
ν_{38}	829	0.498	833	0.955	811	$\delta_{HCH}(54\%)+\gamma_{CCH}(21\%)$ (R3-R4)
ν_{40}	848	1.499	848	0.421	846	$\delta_{HCH}(42\%)+\gamma_{CCH}(35\%)$ (R3-R4)
ν_{41}	858	5.325	856	5.600	858	$\gamma_{CCH}(64\%)+\delta_{OCH}(16\%)$ (R1)
ν_{45}	884	2.107	883	1.821	892	$\delta_{HCH}(56\%)+\delta_{CCH}(19\%)$ (R3-R4)
ν_{46}	918	0.298	913	0.503	906	$\delta_{HCH}(64\%)+\delta_{CCH}(11\%)$ (R3-R4)
ν_{47}	964	1.461	961	1.113	939	$\delta_{HCH}(39\%)+\delta_{CCH}(26\%)+\nu_{CO}(6\%)$
ν_{49}	1010	1.710	1009	0.972	991	$\delta_{HCH}(58\%)+\delta_{CCH}(15\%)$ (R3-R4)
ν_{50}	1032	2.530	1029	2.972	1033	$\delta_{HCH}(57\%)+\delta_{CCH}(17\%)$ (R3-R4)
ν_{51}	1059	2.116	1059	2.007	1051	$\delta_{HCH}(52\%)+\delta_{CCH}(20\%)$ (R3-R4)
ν_{52}	1060	0.612	1062	0.568	1074	$\delta_{HCH}(65\%)+\delta_{CCH}(14\%)$ (R3-R4)
ν_{54}	1102	12.37	1101	11.56	1085	$\delta_{CCH}(49\%)+\nu_{CO}(16\%)$ (R1)
ν_{55}	1104	37.31	1103	37.04	1116	$\tau_{CCCF}(50\%)+\nu_{CF}(34\%)$
ν_{57}	1136	16.11	1135	20.27		$\delta_{HCH}(30\%)+\delta_{CCH}(26\%)+\nu_{CF}(13\%)$
ν_{58}	1153	45.35	1158	39.10	1149	$\delta_{CCH}(32\%)+\delta_{HCH}(27\%)$ (R3)
ν_{59}	1173	2.863	1163	5.110	1168	$\delta_{HCH}(71\%)$ (R3-R4)
ν_{60}	1191	9.412	1190	2.007		$\delta_{HCH}(78\%)$ (R3-R4)
ν_{61}	1195	0.345	1192	5.535	1206	$\delta_{HCH}(70\%)$ (R3-R4)
ν_{66}	1259	3.417	1253	0.997	1253	$\delta_{HCH}(72\%)$ (R3-R4)
ν_{67}	1267	2.477	1274	2.752	1284	$\delta_{HCH}(46\%)+\delta_{CCH}(24\%)$ (R3-R4)
ν_{69}	1314	2.541	1312	6.436	1311	$\delta_{HCH}(65\%)$ (R3)
ν_{74}	1342	4.300	1344	1.966	1350	$\delta_{HCH}(76\%)$ (R3-R4)
ν_{75}	1367	20.40	1365	22.90	1378	$\delta_{CCH}(49\%)+\delta_{HCH}(19\%)$
ν_{79}	1437	0.835	1441	1.135	1433	$\delta_{HCH}(84\%)$ (R4)
ν_{83}	1464	4.300	1467	3.259	1479	$\delta_{HCH}(76\%)$ (R3-R4)
ν_{84}	1501	13.58	1511	18.60	1515	$\delta_{HCH}(48\%)+\nu_{CN}(30\%)$ (R3-R4)
ν_{85}	1531	20.63	1531	18.95	1550	$\nu_{CC}(45\%)+\delta_{CCC}(15\%)+\delta_{CCH}(10\%)$
ν_{86}	1589	63.69	1588	65.60	1596	$\nu_{CC}(30\%)+\delta_{CCC}(23\%)+\delta_{CCH}(15\%)$
ν_{87}	1609	11.28	1611	20.63	1620	$\nu_{CC}(38\%)+\delta_{CCC}(19\%)+\delta_{CCH}(16\%)$
ν_{88}	1760	100	1760	100	1728	$\nu_{CO}(86\%)$ (R1)
ν_{89}	2852	6.923	2869	7.608	2842	$\nu_{CH2}(77\%)$ (Sym) (R3-R4)
ν_{90}	2858	18.71	2874	16.04	2875	$\nu_{CH2}(70\%)$ (Sym) (R3-R4)
ν_{91}	2906	4.162	2902	4.768	2891	$\nu_{CH2}(79\%)$ (Sym) (R3)
ν_{94}	2940	4.475	2934	2.020	2933	$\nu_{CH2}(72\%)$ (Asym) (R3-R4)
ν_{96}	2967	9.592	2947	9.355	2952	$\nu_{CH2}(72\%)$ (Asym) (R3-R4)
ν_{101}	3098	0.340	3099	0.355	3072	$\nu_{CH}(89\%)$ (R1)

ν: stretching; δ: in-plan bending; γ: out-of-plane bending; τ: torsion; *asym*: asymmetric; *sym*: symmetric; R1; Ring 1; R2: Ring 2; R3: Ring 3; R4: Ring 4.
[a]Obtained from the wave numbers calculated at B3LYP/6–311G(d,p) using scaling factors 0.9682.
[b]Relative absorption intensities normalized with highest peak absorption equal to 100.
[f]Total energy distribution calculated B3LYP 6–311G(d,p) level, TED less than 10% are not shown.

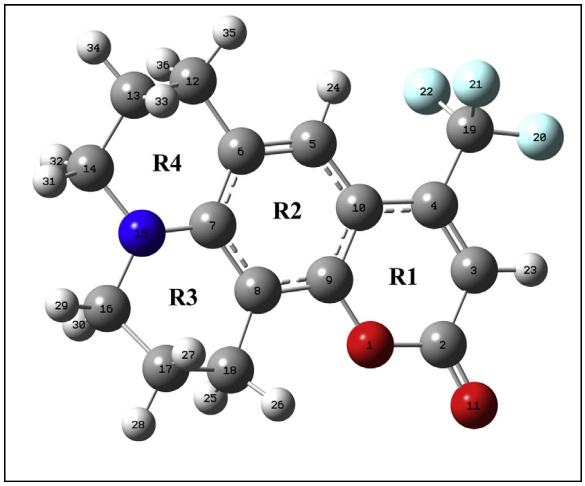

Fig. 2. Optimized structure and atom numbering for Coumarin-153.

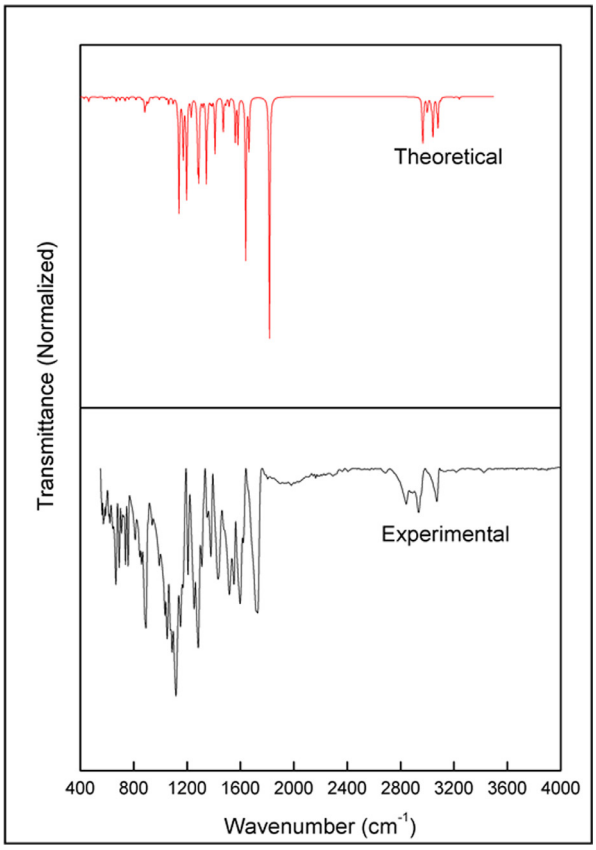

Fig. 3. FT-IR spectra of Coumarin-153 molecule.

stretching band are observed in the region 1870–1540 cm^{-1} [35]. Very strong absorption at 1728 cm^{-1} in IR is assigned to $C = O$ stretching for the Coumarin-153 molecule. The $C = O$ vibration is computed at 1760 cm^{-1} by B3LYP/6–311G(d,p) method show good agreement with the experimental values. The structure of Coumarin-102 is very similar to that of Coumarin-153. When the methyl group of the Coumarin-102 molecule are changed by trifluoromethyl group, the molecule is called Coumarin-153. Zhao and Han et al. [36] reported that the $C = O$ stretching vibration of Coumarin-102 was observed at 1735 cm^{-1} as a very strong absorption band by the FT-IR spectrum. The $C = O$ stretching band is shifted from 1728 cm^{-1} in the Coumarin-153 to 1735 cm^{-1} in the Coumarin-102 molecule.

The vibrational spectral peaks of the experimental IR absorbance [1522, 1596, 1622 cm^{-1}] spectra of the investigated Coumarin-153 are assigned to the Carbon-Carbon stretching vibrations. These vibrations were predicted at 1531, 1589, 1609 cm^{-1} by B3LYP calculation. According to the PED results, these vibrations were estimated as mixed CCC and CCH bending vibrations.

Trifluoromethyl group has the four fundamental vibrations. Beg et al. [37] reported that the symmetric/ anti-symmetric CF_3 stretching vibrations observed at about 1100 cm^{-1}/ 1180 cm^{-1}. In the same work, the symmetric/anti-symmetric CF_3 deformation vibrations appeared at about 700 cm^{-1}/ 520 cm^{-1}. While the symmetric CF_3 stretching vibration appeared at 1116 cm^{-1} in the FT-IR spectra, asymmetric CF_3 stretching vibration couldn't be detected in the FT-IR spectra.

The principal CH_2 vibrations are able to scissoring, wagging, twisting and rocking obtained in the frequency between 1500 cm^{-1} and 800 cm^{-1} [38–40]. CH_2 scissoring vibrations were seen at 1515 cm^{-1}, 1479 cm^{-1} and 1434 cm^{-1} for Coumarin-153 in the infrared spectrum. These vibrational modes were calculated at 1501 cm^{-1} (conformer-1) / 1511 cm^{-1} (conformer-2), 1464 cm^{-1} (conformer-1) / 1467 cm^{-1} (conformer-2) and 1437 cm^{-1} (conformer-1) / 1441 cm^{-1} (conformer-2). The frequencies measured at 1379 cm^{-1} and 1352 cm^{-1} were attributed to the CH_2 wagging modes. According to the DFT results, the CH_2 wagging modes were predicted at 1367 cm^{-1} (conformer-1) / 1365 cm^{-1} (conformer-2) and 1342 cm^{-1} (conformer-1) / 1344 cm^{-1} (conformer-2) by B3LYP/6–311G(d,p) level of theory. The bands at 1311 cm^{-1}, 1284 cm^{-1} and 1253 cm^{-1} in the infrared spectrum, were assigned to the CH_2 twisting mode in the Coumarin-153 molecule. Correspond predicted vibrational modes were calculated at 1314 cm^{-1} (conformer-1) / 1312 cm^{-1} (conformer-2), 1267 cm^{-1} (conformer-1) / 1274 cm^{-1} (conformer-2) and 1259 cm^{-1} (conformer-1) / 1253 cm^{-1} (conformer-2) by B3LYP calculation. Rocking vibrations of the Coumarin-153 molecule seen at 1149 cm^{-1}/1153 cm^{-1} (conformer-1) and 1158 cm^{-1} (conformer-2), 1168 cm^{-1}/1173 cm^{-1} (conformer-1) and1163 cm^{-1} (conformer-2) and 1206 cm^{-1}/1195 cm^{-1} (conformer-1) and 1192 cm^{-1} (conformer-2) in the infrared spectra/theoretical result.

3.3. Nuclear magnetic resonance spectra (NMR)

Using optimized geometry of the Coumarin-153, theoretical ^1H and ^{13}C NMR data were predicted by means of GIAO method. The computed and detected ^1H and ^{13}C data were tabulated in Table 2 in a chloroform solvent. The experimental NMR spectra were illustrated in Fig. 4.

The carbon chemical shift values generally appear in the region of 100 to 150 ppm [41–42]. In the coumarin ring, the experimental shift of the C_4 and C_3 and atoms were measured at 142.0 ppm and 106.5 ppm. The signs of C_7 (δ_C 146.5), C_8 (δ_C 118.9), C_{10} (δ_C 102.4) C_5 (δ_C 127.6) and C_6 (δ_C 123.9) from coumarin, are characteristic for the benzene ring from the benzopyran nucleus. The theoretical values of ^{13}C NMR chemical shifts of the above atoms were determined at the range from 106.3 ppm to 150.6 ppm. The calculated chemical shifts are in good agreement with the experimental values. In Coumarin-153, the carbons C_{14}, C_{16}, C_{12}, C_{13}, C_{17} and C_{18} feature signs δ_C 49.90 ppm, δ_C 49.50, δ_C 27.70 ppm, δ_C 21.20 ppm, δ_C 21.20 ppm and δ_C 20.30 ppm, respectively, indicating that they are methylene. These signals of the conformer-1/conformer-2 were computed at 52.27/51.21 ppm, 51.68/50.95 ppm, 30.52/30.88 ppm, 23.68/23.76 ppm, 23.43/22.66 ppm and 22.76/22.56 ppm by means of DFT.

The C_2 atom has a most shielded signal because C_2 atom is attached to an electronegative oxygen atom O_{11}. The experimen-

Table 2
^{1}H and ^{13}C NMR data of Coumarin-153 compound.

	Theoretical		Experimental		Theoretical		Experimental
Atoms	Conformer-1	Conformer-2		Atoms	Conformer-1	Conformer-2	
C_2	160.8	160.8	160.9	H_{24}	7.22	7.19	7.26
C_9	158.6	158.4	152.0	H_{23}	6.01	5.95	6.31
C_7	152.1	150.5	146.5	H_{32}	3.29	3.28	3.32
C_4	146.6	146.6	142,0	H_{30}	3.28	3.28	3.30
C_{19}	131.4	131.4	141,6	H_{26}	3.12	3.26	3.28
C_5	127.3	126.8	127.6	H_{31}	3.04	3.12	3.26
C_6	123.3	123.0	123.9	H_{29}	3.01	3.11	2.79
C_8	111.8	110.7	118.9	H_{36}	2.76	2.67	2.77
C_3	108.5	107.3	106.5	H_{35}	2.67	2.64	2.77
C_{10}	107.3	106.2	102.4	H_{25}	2.52	2.36	2.75
C_{14}	52.27	51.21	49.9	H_{28}	1.88	1.86	1.99
C_{16}	51.68	50.95	49.5	H_{33}	1.84	1.80	1.97
C_{12}	30.52	30.88	27.7	H_{27}	1.80	1.66	1.95
C_{13}	23.68	23.76	21.2	H_{34}	1.79	1.64	1.93
C_{18}	23.43	22.66	21.2				
C_{17}	22.76	22.56	20.3				

tal signal of C_2 atom is observed at 160.9 ppm for Coumarin-153 molecule. The calculated value noticed that 160.8 ppm for Coumarin-153 by DFT calculations. The experimental signal of C_9 atom, which is connected to the oxygen atom O_1 in the ring, is measured at 152.0 ppm for Coumarin-153. The predicted value notes that 158.6/158.4 ppm for conformer-1/conformer-2 by DFT.

Fluorine atom has also more electronegative property than oxygen and other atoms. So, the C_{19} chemical shift of Coumarin-153 molecule expects to be bigger than ones of other carbon atoms. But, C_{19} chemical shift smaller measured than ones of the carbon atoms, which are connected to the Oxygen atoms of the Coumarin-153 molecule. Because fluorine atoms highly sensitive to magnetic field, some uncounted effects exist in fluorine substituted molecules. In the Coumarin-153 molecule, 131.4 ppm (theoretical) and 141.6 ppm (experimental) signals determined in the NMR spectra [43–44].

Similarly, the aromatic ^{1}H NMR signals in the benzene rings are observed between 7 and 8 ppm [45]. The ^{1}H NMR signal of the benzene ring from the benzopyran nucleus was experimentally observed at 7.26 ppm and theoretically at 7.22/7.19 ppm for conformer-1/conformer-2. Other ^{1}H NMR signal of the benzopyran nucleus was experimentally detected at 6.31 ppm and theoretically at predicted at 6.01/5.95 ppm for conformer-1/conformer-2. These peaks are belonging to the ^{1}H NMR signal of −CH group protons. Other ^{1}H NMR signals are possess $-CH_2$ group protons. The ^{1}H NMR signals of −CH group protons are bigger than those of $-CH_2$ group protons. The $-CH_2$ group protons were grouped as Group 1 (H_{29}, H_{30}, H_{31} and H_{32}), Group 2 (H_{25}, H_{26}, H_{35} and H_{36}) and Group 3 (H_{27}, H_{28}, H_{33} and H_{34}). The sequence of the C_{13} chemical shifts of Groups is the Group 1 >Group 2>Group 3. Because, Group 1 is closer to the electron donating environment than those of the Group 2 and Group 3. The ^{1}H chemical shifts were experimentally measured at 3.32 ppm-3.26 ppm for Group 1, at 2.79 ppm – 2.75 ppm for Group 2 and at 1.99 ppm - 1.93 ppm for Group 3.

3.4. Ultra-violet (UV) spectroscopy analysis

Ultraviolet spectrum analyses of Coumarin-153 were investigated theoretically and experimentally. The methanol with purity (99.9%) was theoretically and experimentally used as a solvent in the present work. From the optimized structure of the conformers, TD-DFT/B3LYP/6–311 G (d, p) computations have been performed to calculate the wavelengths, excitation energies and oscillator strengths in methanol (IEF-PCM solvent method). Computed and detected UV–Vis spectra of Coumarin-153 were given in Fig. 5. The computed and detected data of electronic absorption properties of Coumarin-153 such as the absorption maxima wavelengths (λ_{max}) [44], electronic excitation energies, excited state and oscillator strengths were gathered in Table 3.

Mühlpfordt et al. [46] reported that the lowest excited singlet states of Coumarin-153 molecule, which is names the fluorinated Coumarin-102, given at 3.17 eV (S1 state), 3.86 eV (S2 state), 4.25 eV (S3 state), 4.69 eV (S4 state), 4.79 eV (S5 state), 5.20 eV (S6 state), 5.80 eV (S7 state) and 5.93 eV (S8 state) by using the DFT calculation. All of these reported as μ to μ^* transition. In that study, S1 state is dominated by the HOMO > LUMO excitation. In present work, the first excited state were determined at 405.13 nm (3.0604 eV) for conformer-1 and 406.94 nm (3.0468 eV) for conformer-2 by DFT. Its major contribution is HOMO->LUMO (69%) for both conformer, including excitation from π to π^*. This state (S1) experimentally observed at 422 nm.

Experimentally measured at 266 nm wavelength were predicted at 264.72 nm (4.6837 eV) for conformer-1 and 263.47 nm (4.7059 eV) for conformer-2 by DFT. Its major contribution were obtained the H-3>LUMO (69%). The 214.65 nm (5.7761 eV) for conformer-1 and 215.79 nm (5.7455 eV) were predicted the wavelength in methanol solvent by B3LYP/6–311G(d,p) level of theory. Its major contribution H-1>$L+1$ (52%) for conformer-1 and HOMO>$L+2$ for conformer-2 and the corresponding experimental in methanol has maximum wavelength at 216 nm. The remaining theoretical values are tabulated in Table 3. The agreement between theory and experiment is good. Because, the differences of all band maxima found experimentally are about 0.15 - 0.20 eV of the theoretical values.

3.5. Thermogravimetric and differential thermal analysis (TGA/DTA)

The information about thermal stability of Coumarin-153 obtained by means of Thermogravimetric analysis (TGA) and Differential thermal analysis (DTA) and Differential Thermogravimetric Analysis (DTG). In this experiment, Coumarin-153 was used powder form. The TGA/DTA/DTG curves of the complex were shown in Fig. 6. The temperature of the samples was increased from 30 °C to 550 °C with a heating rate of 10 °C per minute through the programmed dynamic temperature change. In this process, the experiment was carried out in a nitrogen atmosphere at a flow rate of 100 mL/min. There is no temperature difference until the sample undergoes an exothermic or endothermic chemical reaction or change of physical state.

The DTA curve of the Coumarin-153 molecule shows one endothermic peak and one inflexion point. The DTA curve exhibits an endothermic peak at 165 °C. It is representing melting of the

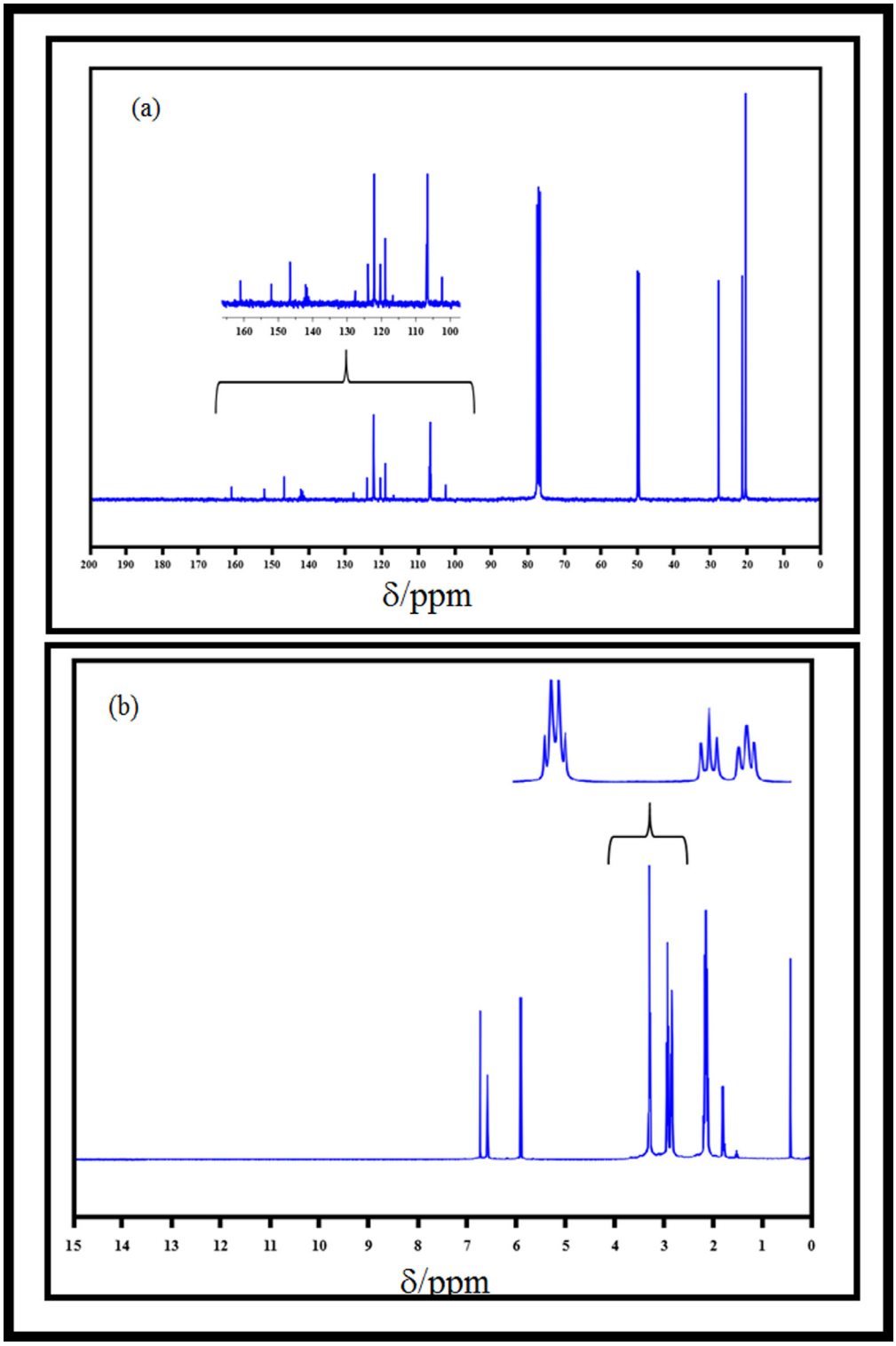

Fig. 4. ^{1}H and ^{13}C NMR spectra of Coumarin-153 molecule.

Coumarin-153 in the lower temperatures. At this temperature, the sample temperature has departed from the baseline and then has returned to the baseline when the reaction or transformation is complete. Also, the inflexion point of the Coumarin-153 appears at 328 °C in the DTA curve. The TGA curve shows continuous weight loss up to 275 °C without any inflexion point. The first inflexion point appears at 315 °C with a weight loss of 89% representing the elimination of Coumarin-153. When mass loss is more readily evaluated from the integral curve, DTG curves always accompany a TGA curves. From the DTG curve, it was observed that Coumarin-153 showed one weight loss at 311 °C. DTG curve has the two very small peak at 166 °C and 222 °C.

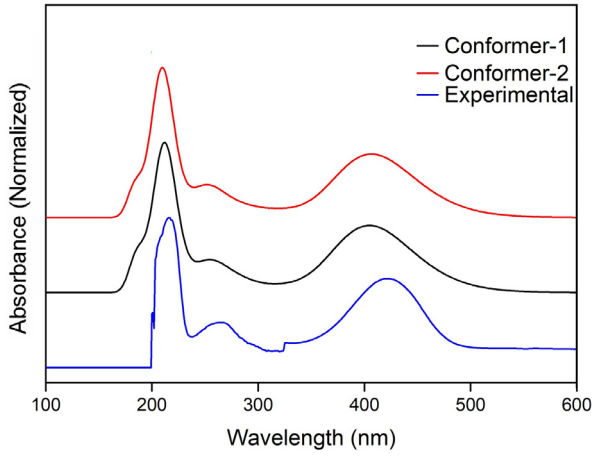

Fig. 5. UV–Vis spectra of Coumarin-153 molecule.

3.6. Molecular electrostatic potential mapped

The experimental results concerning the surface and intermolecular interaction etc. are theoretically supported through the molecular electrostatic potential and electron density counter plots presented in Fig. 7 [47–50]. The MEP contours and surfaces have been established extensively as a guide to the interpretation and prediction of molecular behavior. This map surface and counter shows the varied charged areas of a molecule, pointing out the role of the molecular reactivity. The MEPs are either negative, low potentials that are characterized by an abundance of electrons and reactive with electrophiles, or positive, high potentials that are characterized by an absence of electrons and reactive with nucleophiles. The MEP plot of Coumarin-153 reveals that the $C = O$ group of the benzopyran nucleus exert the most negative potential. In this sense, the maximum negative region, indicated as dark red color, is the preferred site for an electrophilic attack, so that, the $C = O$ group will be closer to the surface, other molecules etc.

3.7. Frontier molecular orbital analysis (FMO)

The highest occupied molecular orbital (HOMO) and lowest unoccupied molecular orbital (LUMO) are a very important parameters for both chemists and physicists. In DSSCs, one of the most important characters of dye molecules are HOMO and LUMO levels. According the Structure and working principle of DSSC, excited state level (LUMO) of the molecule should be appropriately higher than the conduction band edge of used semiconductor. However, ground state level (HOMO) of the molecule has to be sufficiently lowers than the redox potential to regenerate the oxidized dye.

As shown in Fig. 8, the HOMO has strong contributions over the whole molecule without the trifluoromethyl group. The LUMO is localized on the quinolizidine ring, nitrogen atom and trifluoromethyl group. When HOMO-LUMO excitation is stimulated with light radiation, this stimulation caused the electron distribution to shift from quinolizidine rings to the right side of the molecule. It's may be noted that the photo induced charge transfer from the coumarin derivatives to the TiO_2 electrode could happen effectively by the HOMO-LUMO transition.

As seen in Table 4, its note that the LUMO energies of Coumarin-153 were predicted at −1.810 eV, which is far above the conduction band of TiO_2. However, the HOMO energy of the redox couple (I^-/I_3^-) reported as −4.8 eV. The HOMO energy of Coumarin-153 were predicted as −5.405 eV by DFT. The HOMO energy of Coumarin-153 appears to be lower than that of redox couple. It can also be found in Table 4 that the HOMO-LUMO gap of Coumarin-152 is lower than that of Coumarin-102. So, Coumarin-153 would be more productive than Coumarin-102 for DSSC [51].

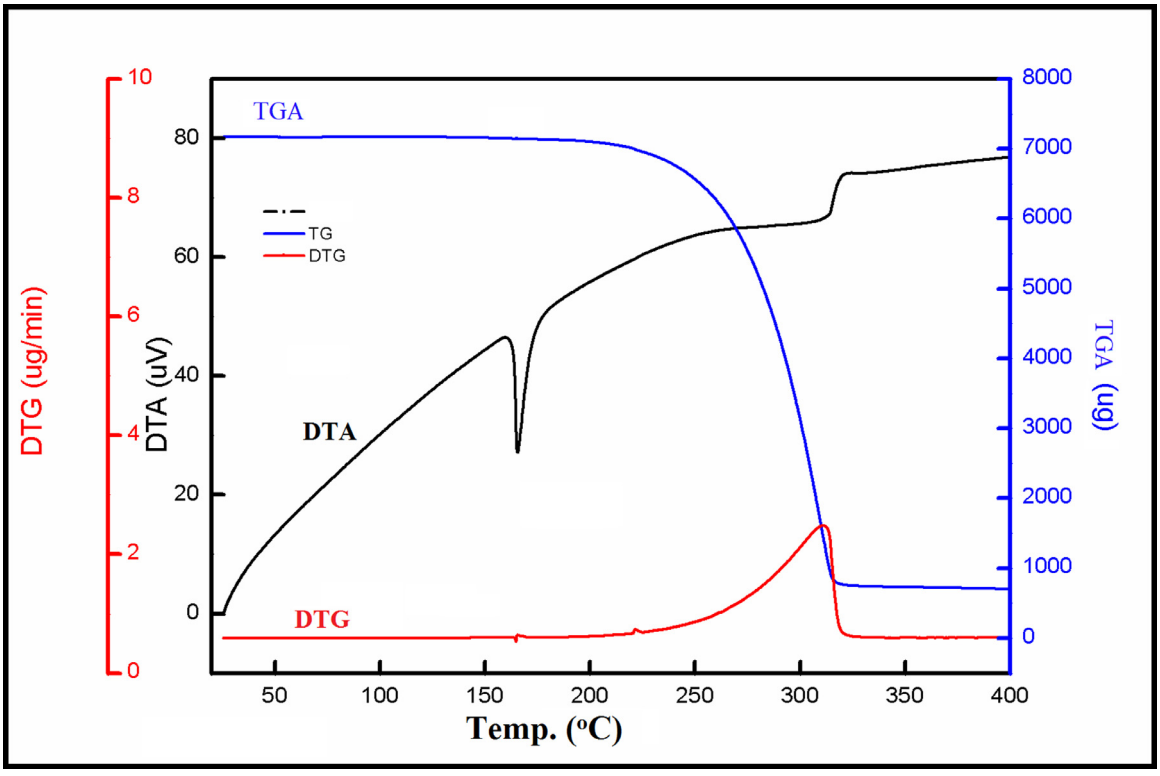

Fig. 6. TGA, DTG and DTA curves of Coumarin-153 molecule.

Table 3
Uv-Vis spectral data of conformers of Coumarin-153 compound.

	Wavelength λ (nm)	Excitation energies (eV)	Excited state	Oscillator strengths (f)
Conformer-1	405.13 (422)*	3.0604	HOMO>LUMO(69%)	0.3931
	330.19	3.7550	H-1>LUMO(69%);HOMO>*L* + 1(11%)	0.0367
	283.46	4.3740	H-1>LUMO(12%);H-1>*L* + 2(13%);HOMO>*L* + 1(67%)	0.0589
	264.72 (266)*	4.6837	H-3>LUMO(69%)	0.0002
	257.51	4.8147	H-2>LUMO(25%);HOMO>*L* + 2(64%)	0.1333
	243.30	5.0960	H-2>LUMO(62%);H-1>*L* + 2(16%);HOMO>*L* + 2(22%)	0.0648
	214.65 (216)*	5.7761	H-1>*L* + 1(52%);H-1>*L* + 2(33%);HOMO>*L* + 3(25%)	0.4886
	212.71	5.8289	H-2>*L* + 1(17%);H-1>*L* + 1(18%);H-1>*L* + 2(50%);HOMO>*L* + 3(38%)	0.0763
	210.29	5.8959	H-7>LUMO(11%);H-4>LUMO(63%);HOMO>*L* + 3(22%)	0.0266
	208.66	5.9418	H-5>LUMO(21%);H-4>LUMO(20%);H-1>*L* + 1(35%);H-1>*L* + 2(18%);HOMO>*L* + 3(46%)	0.2960
	200.33	6.1890	H-6>LUMO(11%);H-5>LUMO(61%);H-2>*L* + 1(22%);H-1>*L* + 1(14%)	0.0312
	196.11	6.3223	HOMO>*L* + 4(69%)	0.0255
	194.92	6.3606	H-10>LUMO(14%);H-7>LUMO(11%);H-6>LUMO(62%);H-5>LUMO(11%);H-4>LUMO(12%)	0.0012
	190.63	6.5039	H-2>*L* + 1(13%);HOMO>*L* + 5(67%)	0.0086
	189.90	6.5290	H-10>LUMO(14%);H-8>LUMO(20%);H-7>LUMO(55%);H-6>LUMO(23%);H-4>LUMO(12%);H-3>*L* + 1(11%)	0.0023
	187.13	6.6256	H-8>LUMO(15%);H-7>LUMO(10%);H-5>LUMO(15%);H-3>*L* + 1(10%);H-2>*L* + 1(56%);H-1>*L* + 2(19%);HOMO>*L* + 5(12%)	0.1713
	186.05	6.6641	H-10>LUMO(16%);H-8>LUMO(17%);H-7>LUMO(29%);H-6>LUMO(11%);H-3>*L* + 1(46%);H-3>*L* + 2(29%)	0.0038
	184.44	6.7221	H-10>LUMO(12%);H-8>LUMO(54%);H-7>LUMO(21%);H-3>*L* + 1(26%);H-3>*L* + 2(14%)	0.0199
	183.41	6.7601	HOMO>*L* + 6(68%);HOMO>*L* + 7(14%)	0.0109
	181.26	6.8400	H-11>LUMO(20%);H-10>LUMO(52%);H-8>LUMO(26%);H-3>*L* + 1(17%);H-2>*L* + 2(16%)	0.0158
Conformer-2	406.94 (422)*	3.0468	HOMO>LUMO(69%)	0.4060
	325.95	3.8038	H-1>LUMO(68%);HOMO>*L* + 1(12%)	0.0416
	283.99	4.3658	H-1>LUMO-(12%);H-1>*L* + 2(12%);HOMO>*L* + 1(67%)	0.0596
	263.47 (266)*	4.7059	H-3>LUMO(69%)	0.0002
	255.27	4.8569	H-2>LUMO(28%);HOMO>*L* + 2(63%)	0.1534
	240.50	5.1649	H-2>LUMO(61%);H-1>*L* + 2(16%);HOMO>*L* + 2(25%)	0.0724
	215.79 (216)*	5.7455	H-1>*L* + 2(20%);HOMO>*L* + 3(65%)	0.0303
	218.70	5.8795	H-1>*L* + 1(52%);H-1>*L* + 2(35%);HOMO>*L* + 3(20%)	0.6540
	209.06	5.9306	H-4>LUMO(57%);H-2>*L* + 1(10%);H-1>*L* + 1(16%);H-1>*L* + 2(28%)	0.0506
	208.41	5.9491	H-5>LUMO(20%);H-4>LUMO(31%);H-2>*L* + 1(17%);H-1>*L* + 1(35%);H-1>*L* + 2(38%)	0.1818
	206.00	6.1808	H-5>LUMO(16%);HOMO>*L* + 4(67%)	0.0591
	197.58	6.2751	H-5>LUMO(59%);H-4>LUMO(16%);H-2>*L* + 1(22%);H-1>*L* + 1(11%);HOMO>*L* + 4(13%)	0.0273
	193.73	6.3999	H-10>LUMO(19%);H-7>LUMO(10%);H-6>LUMO(63%)	0.0002
	191.43	6.4766	HOMO>*L* + 5(68%)	0.0009
	187.89	6.5988	H-10>LUMO(20%);H-7>LUMO(58%);H-6>LUMO(21%);H-4>LUMO(12%);H-3>*L* + 1(14%)	0.0008
	185.54	6.6824	H-10>LUMO(13%);H-5>LUMO(12%);H-3>*L* + 1(25%);H-3>*L* + 2(15%);H-2>*L* + 1(40%);H-1>*L* + 2(13%);HOMO>*L* + 6(38%)	0.0831
	185.37	6.6884	H-10>LUMO(10%);H-7>LUMO(11%);H-3>*L* + 1(20%);H-3>*L* + 2(13%);H-2>*L* + 1(21%);HOMO>*L* + 6(57%)	0.0336
	184.55	6.7181	H-8>LUMO(14%);H-7>LUMO(24%);H-5>LUMO(11%);H-3>*L* + 1(37%);H-3>*L* + 2(25%);H-2>*L* + 1(36%);H-1>*L* + 2(11%)	0.0806
	182.87	6.7799	H-10>LUMO(13%);H-8>LUMO(59%);H-3>*L* + 1(10%);HOMO>*L* + 7(27%)	0.0171
	182.41	6.7969	H-8>LUMO(26%);HOMO>*L* + 7(61%);HOMO>*L* + 9(14%)	0.0009

H:HOMO, L: LUMO.
*Experimental data.

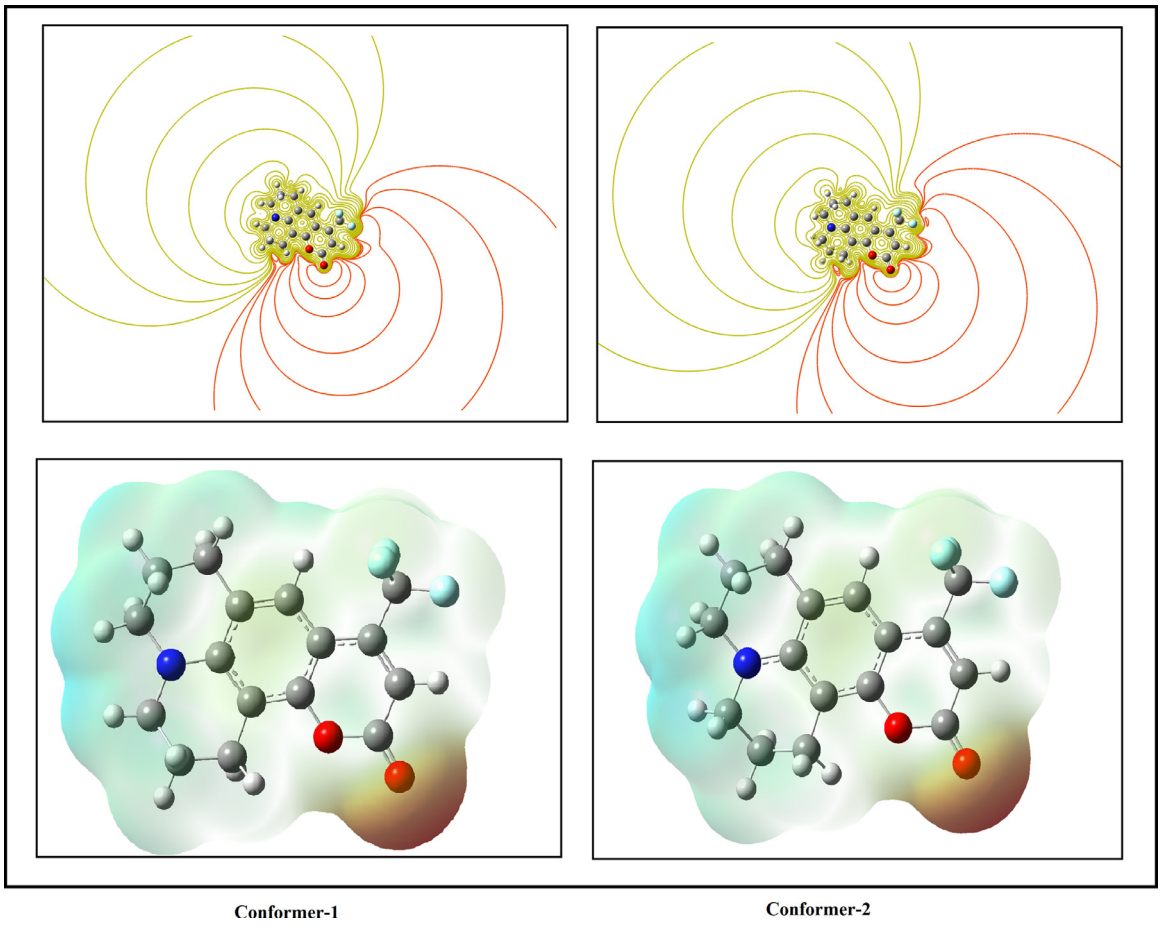

Fig. 7. Molecular electrostatic potential mapped on to isodensity surface.

Table 4
Some chemical reactivity parameters of Coumarin-153 compound.

	Coumarin153	Coumarin 102
ΔE_{LUMO}	−1.810	−1.351
ΔE_{HOMO}	−5.405	−5.059
$\Delta E_{HOMO\text{-}LUMO}$	3.595	3.027
I_P (eV)	5.405	5.059
E_A (eV)	1.810	1.351
χ (eV)	3.607	3.205
η (eV)	1.797	1.854
S $(eV)^{-1}$	0.278	0.269
ω (eV)	3.620	2.770
μ (Debye)	7.016	9.144

3.8. Some selected electronic properties

HOMO energy is characterized as electron donating ability. LUMO energy is characterized as the ability to obtain electron. The LUMO energy levels are sufficiently high to provide the driving force for electron injection from the excited dye molecules. The HOMO-LUMO gap energies display the possibility of electron excitation and transportation in DSSCs. Besides, the energy gap between HOMO-LUMO energy levels provides some information such as stability, polarizability, chemical hardness and chemical softness of the molecules. For example, wide HOMO-LUMO gap express high stability, while narrow HOMO-LUMO gap are associated with low stability. Similarly, when HOMO-LUMO gap of the molecule is large, it is a hard molecule. It is a soft molecule when the HOMO-LUMO gap of the molecule is small. As a result, the soft molecules will be more reactive than hard molecules for unimolecular reactions.

As seen in Table 4, $\Delta E_{HOMO\text{-}LUMO}$ gap value of conformer-1 of the Coumarin-153 estimated bigger than that of Coumarin-102. Therefore, Coumarin-153 molecule is the hardest than Coumarin-102 molecule. In addition to, the HOMO-LUMO energy value of the urea molecule was reported at 6.706 eV [52]. The HOMO-LUMO energy value of the urea molecule bigger than those of Coumarin-153 and Coumarin-102 molecules. So, its note that the Coumarin-102 and Coumarin-153 molecules are more polarizable than the urea.

Ionization potential (IP), which is directly dependent HOMO energy, is the minimum energy required to remove an electron from the molecule. Electron affinity (EA), which is directly dependent LUMO energy, is the minimum energy required to add electrons to the molecule. The chemical hardness and softness are directly related to ionization potential and electron affinity. The chemical hardness and softness is a term related to preventing intermolecular charge transfer [53]. In the conformer-1 of Coumarin-153 molecule, the IP value was computed at 5.405 eV by DFT. Pryor et al. [54] reported that ionization potential (Ip) of the Coumarin-153 molecule at 7.21 eV by using the UV experimental. The EA value was obtained at 1.810 eV by DFT.

The dipole moment of Coumarin-102 measured at 6.98 Debye in the chloroform environment [9]. Cave et al. [55] reported that the dipole moment of the Coumarin-102 molecule predicted at 6.81 Debye, 5.99 Debye and 7.16 Debye for PBE0/6–311G(d,p), MP2/6–311G(d,p) and RHF/6–311G(d,p), respectively. In that work, the dipole moment of Coumarin-153 molecule determined at 6.55

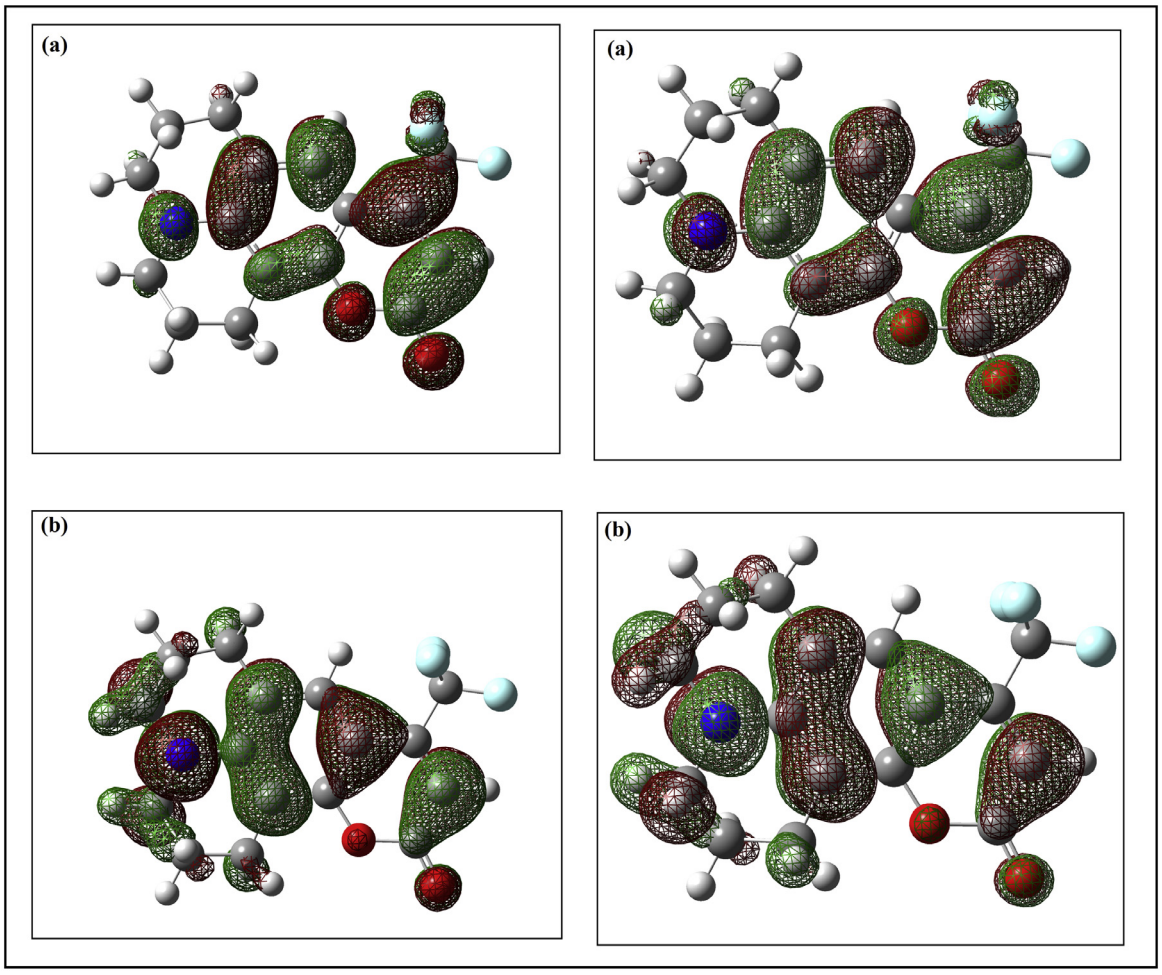

Fig. 8. HOMO (b) –LUMO (a) plots of Coumarin-153 molecule.

Table 5
Antimicrobial activity of compounds and standard reagents (diameter of zone inhibition (mm)).

COMPOUNDS	Coumarin 153	AMP 10	SXT 25	AMC 30	K 30	NYS 100	
Gram (+)	*Micrococcus luteus*	17	22	21	25	23	N
	Staphylococcus epidermis	21	26	25	27	25	N
	Staphylococcus aureus	–	30	24	30	25	N
	Bacillus cereus	16	23	25	20	28	N
Gram (-)	*Pseudomonas putida*	15	8	18	15	14	N
	Klebsiella pneumonia	17	21	20	21	23	N
	S. typhi H	16	11	17	19	20	N
	E. coli	19	10	18	14	25	N
	Proteus vulgaris	18	17	19	20	21	N
Yeast	*Candida albicans*	16	N	N	N	N	20

N: Not determined, AMP10 (ampicillin 10 μg), SXT25 (sulfamethoxazole 25 μg), AMC30 (amoxycillin 30 μg), K30 (kanamycin 30 μg), NYS100 (nystatin 100 μg).

Debye (experimental), 7.24 Debye (PBE0/6–311G(d,p)) and 6.43 Debye (MP2/6–311G(d,p)). In the present work, the dipole moment of conformer-1 of the Coumarin-153 molecule given at 7.016 Debye for B3LYP/6–311G(d,p) level of theory. These results could be of interest as an indication of the solubility and chemical reactivity of the studied molecule, not only for it synthesis but for the potential application in organic electronics and photovoltaics.

The biological activity can be described using the electrophilicity index. For the conformer-1 of Coumarin-153 molecule, the electrophilicity index was predicted at 3.620 eV. It can be stated that the Coumarin-153 molecule is biologically active [56–57].

4. Anti-Microbial activity

The antifungal and antibacterial activities for Coumarin-153 molecule are presented in Table 5 and Figure S1. The Coumarin-153 was screened for in vitro antibacterial and antifungal activity in DMF as a test substance. The Coumarin-153 was tested with the same concentrations in DMF solution (0.25 µg/µL). The Coumarin-153 and antibiotics indicated varying degrees of inhibitory effects on the growth of different tested both Gram-negative and Gram-positive pathogenic bacteria and yeast (Table 5). The Coumarin-153 was more effective in Gram-positive bacteria than Gram-

negative bacteria (Table 5). Coumarin-153 showed the most activity against *Staphylococcus epidermis* (21 mm) than commercial (standard) antibiotics (positive control) (Table 5). *Staphylococcus epidermis* infections are associated with intravascular devices (prosthetic heart valves, etc.), but are often seen in patients with prosthetic joints, large wounds and catheters. These pathogenic microorganisms continue to gain resistance to conventional antibiotics [58]. In addition, antibacterial activity of Coumarin-153 compared with seven commercial antibiotics. Authors note that the Coumarin-153 were as effective as the antibiotics mentioned.

5. Conclusion

- ü A joint vibrational, NMR and UV–Vis spectroscopy and quantum chemistry study has been carried out to investigate the Coumarin-153 molecule. The results of the theoretical spectroscopic calculations showed that good agreement with the experimental values.
- ü The first excited state of Coumarin-153 was theoretically and experimentally determined at 406.94 nm and 422 nm, respectively. This state is dominated by the HOMO -> LUMO excitation, including excitation from π to π^*.
- ü The information about thermal stability of Coumarin-153 obtained by means of TGA and DTA and DTG. The TGA curve showed that the first inflexion point appears at 315 °C with a weight loss of 89% representing the elimination of Coumarin-153. The DTA curve of the Coumarin-153 molecule shows one endothermic peak at 165 °C and one inflexion point at 328 °C. The DTG curve of Coumarin-153 showed one weight loss at 311 °C and two very small peak at 166 °C and 222 °C.
- ü In DSSCs, one of the most important characters of dye molecules are HOMO and LUMO levels. The HOMO has strong contributions over the whole molecule without the trifluoromethyl group. The LUMO is localized on the benzene ring, pyrone ring, and trifluoromethyl group.
- ü It can be said that the Coumarin-153 molecule is biologically active, because the electrophilicity index of the Coumarin-153 were calculated at 4.044 eV.
- ü The Coumarin-153 and antibiotics indicated varying degrees of inhibitory effects on the growth of different tested both gram negative and gram positive pathogenic bacteria and yeast. The Coumarin-153 was more effective in gram-positive bacteria than gram-negative bacteria. Its note that it's showed the most activity against Staphylococcus epidermis than commercial antibiotics.

Declaration of Competing Interest

The authors declare that they have no known competing financial interests or personal relationships that could have appeared to influence the work reported in this paper.

CRediT authorship contribution statement

Y. Erdogdu: Supervision, Investigation, Writing - review & editing. **U.C. Baskose:** Formal analysis, Writing - review & editing. **S. Saglam:** Supervision, Investigation, Methodology. **M. Erdogdu:** Investigation, Validation. **H. Ogutcu:** Investigation, Validation. **S Özçelik:** Investigation, Validation.

Acknowledgements

Thanks to Dr. Yıldırım AYDOĞDU for Thermogravimetric and Differential thermal analysis measurements. In addition, thanks to Dr. M. ERDOGDU and Dr. H. ÖGÜTÇÜ for anti-microbial study. This study was supported by Gazi University Scientific Research Projects Department (BAP project code: 05/2018–05).

Supplementary materials

Supplementary material associated with this article can be found, in the online version, at doi:10.1016/j.molstruc.2020.128873.

References

[1] R.V. Fernandes, A. Urbano, J.L. Duarte, N. Bristow, J. Kettle, E. Laureto, J. Lumin. 203 (2018) 165–171.
[2] P.C. Ricci, A. Da Pozzo, S. Palmas, F. Muscas, C.M. Carbonaro, Chem. Phys. Lett. 531 (2012) 160–163.
[3] J. Gong, K. Sumathy, Q. Qiao, Z. Zhou, Renew. Sustain. Energy Rev. 68 (2017) 234–246.
[4] D.G. Mitnik, J. Mol. Struct. Theochem. 911 (2009) 105–108.
[5] M. Grätzel, J. Photochem. Photobiol. C 4 (2003) 145–153.
[6] L. Lu, J. Chen, L. Li, W. Wang, Nanoscale Res. Lett. 7 (2012) http://www.nanoscalereslett.com/content/7/1/293.
[7] Y.Lee Birkel, D. Koll, X.V. Meerbeek, S. Frank, M.J. Choi, Y.S. Kang, K. Char, W. Tremel, Energy Environ. Sci. 5 (2012) 5392–5400.
[8] S. Gubbala, V. Chakrapani, V. Kumar, M.K. Sunkara, Adv. Funct. Mater. 18 (2008) 2411–2418.
[9] M. Ye, X. Wen, M. Wang, J. Iocozzia, N. Zhang, C. Lin, Z. Lin, Mater. Today 18 (2015) 155–162.
[10] M. Katsori, D.H. Litina, Expert Opin. Ther. Pat. 24 (2014) 1323–1347.
[11] T. Nasr, S. Bondock, M. Youns, Eur. J. Med. Chem 76 (2014) 539–548.
[12] D. Maity, D. Karthigeyan, T.K. Kundu, T. Govindaraju, Sens. Actuators B 176 (2013) 831–837.
[13] K.K. Upadhyay, R.K. Mishra, A. Kumar, J.Z. Zhao, R.J. Prasad, J. Mol. Struct. 963 (2010) 228–233.
[14] I. Padilla-Martinez, I.Y. Flores-Larios, E.V. Garcia-Baez, J. Gonzalez, A. Cruz, F.J. Martinez-, Martinez, Mol. 16 (2011) 915–932.
[15] P. Barot, S.V. Jain, L. Kremer, S. Singh, M. D.Ghate, Med. Chem. Res. 24 (2015) 2771–2798.
[16] M.J. Frisch, A.B. Nielson, A.J. Holder, Gaussview User Manual, Gaussian Inc., Pittsburgh, PA, 2000.
[17] M.J Frisch, G.W Trucks, H.B Schlegel, G.E Scuseria, M.A Robb, J.R Cheeseman, G Scalmani, V Barone, B Mennucci, G.A Petersson, H Nakatsuji, M Caricato, X Li, H.P Hratchian, A.F Izmaylov, J Bloino, G Zheng, J.L Sonnenberg, M Hada, M Ehara, K Toyota, R Fukuda, J Hasegawa, M Ishida, T Nakajima, Y Honda, O Kitao, H Nakai, T Vreven, J.A Montgomery Jr, J.E Peralta, F Ogliaro, M Bearpark, J.J Heyd, E Brothers, K.N Kudin, V.N Staroverov, R Kobayashi, J Normand, K Raghavachari, A Rendell, J.C Burant, S.S Iyengar, J Tomasi, M Cossi, N Rega, J.M Millam, M Klene, J.E Knox, J.B Cross, V Bakken, C Adamo, J Jaramillo, R Gomperts, R.E Stratmann, O Yazyev, A.J Austin, R Cammi, C Pomelli, J.W Ochterski, R.L Martin, K Morokuma, V.G Zakrzewski, G.A Voth, P Salvador, J.J Dannenberg, S Dapprich, A.D Daniels, Ö Farkas, J.B Foresman, J.V Ortiz, J Cioslowski ve, D.J FoxGaussian 09, Revision B.01, Gaussian Inc, 2010 Wallingford CT.
[18] A.D. Becke, Phys. Rev. A 38 (1988) 3098–3100.
[19] R. Krishnan, J.S. Binkley, R. Seeger, J.A. Pople, J. Chem. Phys. 72 (1980) 650.
[20] G. Rauhut ve, P. Pulay, J. Phys. Chem. 99 (1995) 3093–3100.
[21] H. Öğütçü, N. Kurnaz Yetim, E. Hasanoglu Özkan, O. Eren, G. Kaya, N. Sarı, A. Dişli, P.J. Chem, Techn 19 (2017) 74–80.
[22] U. Schillinger, F.K. Lucke, Appl. Environ. Microbiol. 55 (1989) 1901–1906.
[23] C. Nithya, B. Gnanalakshmi, S.K. Pandian, Mar. Environ. Res. 71 (2011) 283–294.
[24] E. Bozkır, N. Sarı, H. Ögütcü, J. Inorg. Organomet. Pol. and Mat. 22 (2012) 1146–1155.
[25] N. Sarı, N. Pişkin, H. Öğütcü, N. Kurnaz, Med. Chem. Res. 22 (2013) 580–587.
[26] D. Nartop, N. Sarı, Chin H.Öğütcü, J. Inorg. Chem 30 (2014) 921–939.
[27] M. Çınarlı, Ç.Yüksektepe Ataol, H. Bati, F. Güntepe, H. Ögütçü, O. Büyükgüngör, Inorganica Chim. Acta 484 (2019) 87–94.
[28] S. Koçoğlu, H. Ogutcu, Z. Hayvalı, Res. Chem. Intermed. 45 (2019) 2403–2427.
[29] H.Erdogan Y.Altundas, E.Kizil H.Ögütcü, G. Agar, Fresenius Environ. Bull. 25 (2016) 5411–5418.
[30] F. Altundas, N. Sarı, N. Colak, H. Ögütcü, Med. Chem. Res. 19 (2010) 576–588.
[31] D. Nartop, N. Sarı, A. Altundas, H. Ögütcü, J. Appl. Polym. Sci. 125 (2012) 1796–1903.
[32] S. Ceker, H. Ogutcu, S. Meral, A.A. Agar, G. Agar, Pak. J. Pharm. Sci. 32 (2019) 2679–2686.
[33] B.C. Yip, F.M. Moo, K.S. Lok, H.K. Fun, K. Sivakumar, Acta Crystallogr., Section C: Cryst. Struct. Commun. 52 (1996) 477–481.
[34] M. Tanışlı, N.Şahin E.Taşal, Ç. Arslan, J. Mol. Liq. 240 (2017) 733–751.
[35] M. Silverstein, G. Clayton Basseler, C. Morill, Spectrometric Identification of Organic Compounds, Wiley, New York, 1981.
[36] G.J. Zhao, K.L. Han, J. Phys. Chem. A 111 (2007) 2469–2474.
[37] M.A.A. Beg, H.C. Clark, Can J Chem. 40 (1962) 393–398.
[38] V. Chiş, S. Filip, V. Miclauş, A. Pirnau, C. Tanaselia, V. Almas, M. Vasilescu, J. Mol. Struct. 744-747 (2005) 363–368.
[39] S. Subashchandrabose, V. Thanikachalam, G. Manikandan, H. Saleem, Y. Erdogdu, Spectrochim. Acta Part A 157 (2016) 96–103.
[40] S. Saglam, A. Disli, Y. Erdogdu, M.K. Marchewka, M.T. Güllüoğlu, Spectrochim. Acta Part A 135 (2015) 1011–1018.
[41] H.O. Kalinowski, S. Berger, S. Braun, Carbon-13 NMR Spectroscopy, John Wiley & Sons, ltd, 1988.

[42] K. Pihlaja, E. Kleinpeter, Carbon-13 NMR Chemical Shifts in Structural and Stereochemical Analysis, VCH Publishers, New York, 1994.
[43] E. Kose, M. Karabacak, F. Bardak, A. Ataç, J. Mol. Struct. 1123 (2016) 284–299.
[44] A. Atilgan, S. Yurdakul, Y. Erdogdu, M.T. Güllüoglu, J. Mol. Struct. 1161 (2018) 55–65.
[45] L. Xie, Y. Chen, W. Wu, H. Guo, J. Zhao, X. Yu, Dyes Pigm. 92 (2012) 1361–1369.
[46] A. Mühlpfordt, R. Schanz, N.P. Ernsting, V. Farztdinov, S. Grimmeb, Phys. Chem. Chem. Phys. 1 (1999) 3209–3218.
[47] I. Alkorta, J.J. Perez, Int. J. Quantum Chem. 57 (1996) 123–135.
[48] E. Scrocco, J. Tomasi, Advances in Quantum Chemistry, Academic Press, New York, 1978.
[49] F.J. Luque, M. Orozco, P.K. Bhadane, S.R. Gadre, J. Phys. Chem. 97 (1993) 9380–9384.
[50] J. Sponer, P. Hobza, Int. J. Quantum Chem. 57 (1996) 959–970.
[51] S.A. Siddiqui, J. Phys. Org. Chem. 31 (2018) 3905–3915.
[52] S.M. Soliman, M. Hagar, F.S.H. El Ashry, Spectrochimica Acta Part A: molecular and biomolecular spectroscopy. 145 (2015) 270–279.
[53] T.A. Koopmans, Physica 1104 (1933) 113.
[54] B.A. Pryor, P.M. Palmer, Y. Chen, M.R. Topp, Chem. Phys. Lett. 299 (1999) 536–544.
[55] R.J. Cave, Jr, E.W. Castner, J. Phys. Chem. A 106 (2002) 12117–12123.
[56] P. Shafieyoon, E. Mehdipour, Y.S. Mary, J. Mol. Struct. 1181 (2019) 244–252.
[57] Y. Erdogdu, Ş. Yurdakul, S. Badoglu, M.T. Güllüoğlu, J. Mol. Struct. 1184 (2019) 364–374.
[58] S. Koçoğlu, H. Ogutcu, Z. Hayvalı, Res. Chem. Intermed. 45 (2019) 2403–2427.